Cell Metabolism

Article

Mitochondrial lactate venting limits oxidative stress

Graphical abstract

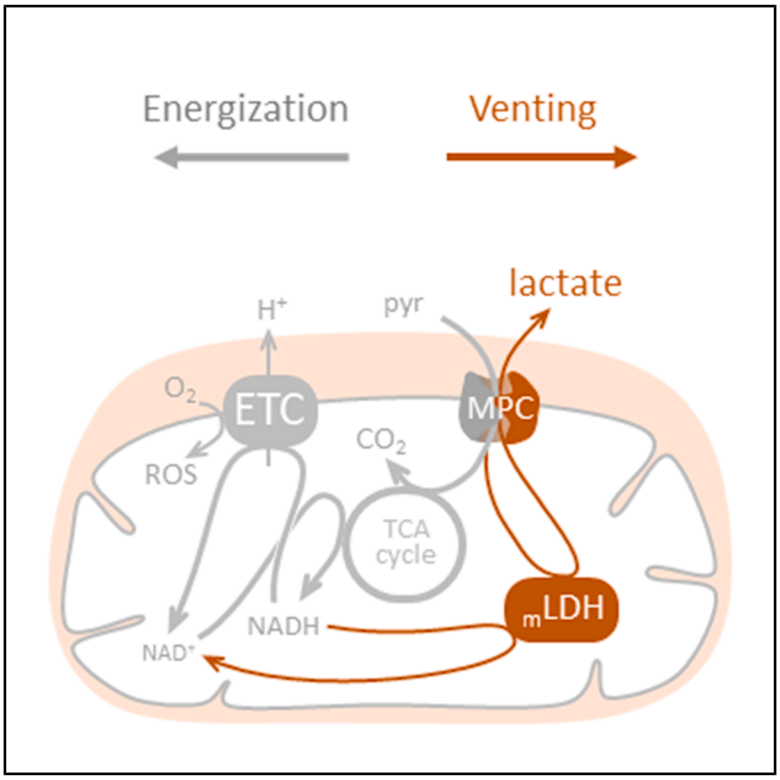

Authors

Daniela Rauseo,
Yasna Contreras-Baeza,
Mildreth Salazar, ..., Bruno Weber,
Pamela Y. Sandoval, L. Felipe Barros

Correspondence

pamela.sandoval@uss.cl (P.Y.S.),
luis.barros@uss.cl (L.F.B.)

In brief

The main function of mitochondria is to generate ATP by oxidizing pyruvate to CO_2. Rauseo et al. show that matrix pyruvate is also converted to lactate, which is released to the cytosol via the MPC to modulate ROS production. Hypoxia increased ROS and boosted the release of lactate by mitochondria.

Highlights

- Mammalian mitochondria are not energized by lactate, they produce it
- Lactate export involves the mitochondrial pyruvate carrier (MPC)
- Lactate production is favored by high matrix NADH levels
- Pharmacological inhibition of lactate export results in matrix ROS accumulation

Rauseo et al., 2026, Cell Metabolism *38*, 1130–1140
June 2, 2026
https://doi.org/10.1016/j.cmet.2026.02.020

CellPress

CellPress

Cell Metabolism

Article

Mitochondrial lactate venting limits oxidative stress

Daniela Rauseo,[1,2,4] Yasna Contreras-Baeza,[1,2,4] Mildreth Salazar,[1,2] Abigail J. Galarza,[1,2] Sebastián Holtheuer-Gallardo,[1,3] Hugo Faurand,[1,2] Natali Cárcamo-Lemus,[1,2] Raibel Suárez,[1,2] Joel L. Asenjo,[4] Alexandra von Faber-Castell,[5,6] Franco Silva,[1,2] Valentina Mora-González,[7] Jan Dernic,[5,6] Luca Ravotto,[5,6] Matthias T. Wyss,[5,6] Felipe Baeza-Lehnert,[9] Iván Ruminot,[1,3] Carlos Alvarez-Navarro,[7,8] Alejandro San Martín,[1,2] Bruno Weber,[5,6] Pamela Y. Sandoval,[1,2,*] and L. Felipe Barros[1,2,10,*]

[1]Centro de Estudios Científicos-CECs, Valdivia, Chile
[2]Facultad de Medicina, Universidad San Sebastián, Valdivia, Chile
[3]Facultad de Ciencias de la Rehabilitación y Calidad de Vida, Universidad San Sebastián, Valdivia, Chile
[4]Universidad Austral de Chile, Valdivia, Chile
[5]Institute of Pharmacology and Toxicology, University and ETH Zurich, Zurich, Switzerland
[6]Neuroscience Center Zurich, ETH and University Zurich, Zürich, Switzerland
[7]Instituto de Inmunología, Facultad de Medicina, Universidad Austral de Chile, Valdivia, Chile
[8]Unidad de Proteómica, AUSTRAL-omics, Universidad Austral de Chile, Valdivia, Chile
[9]Carl-Ludwig-Institute for Physiology, Faculty of Medicine, University of Leipzig, Leipzig, Germany
[10]Lead contact
*Correspondence: pamela.sandoval@uss.cl (P.Y.S.), luis.barros@uss.cl (L.F.B.)
https://doi.org/10.1016/j.cmet.2026.02.020

SUMMARY

Lactate has been proposed to enter mitochondria and fuel respiration, but this "intracellular lactate shuttle" remains controversial. Using genetically encoded lactate and redox sensors in cultured cells and neurons *in vivo*, we identify a dynamic lactate pool within the mitochondrial matrix that tracks extracellular and blood lactate and promotes lactylation of mitochondrial proteins. Lactate crosses the inner mitochondrial membrane through a saturable pathway that is partly sensitive to pharmacologic and genetic inhibition of the mitochondrial pyruvate carrier (MPC). Despite transport and matrix lactate dehydrogenase activity, lactate does not measurably energize the electron transport chain under the conditions tested. Instead, energized mitochondria can produce lactate from pyruvate, a response enhanced by hypoxia. Blocking MPC causes matrix lactate and H_2O_2 accumulation, revealing a rapid lactate-based "vent" that modulates matrix energy and reactive oxygen species.

INTRODUCTION

Mitochondria are energized by pyruvate, which is generated in the cytosol from various sources, including glucose, lactate, and amino acids. Once in the mitochondrial matrix, pyruvate is oxidized to CO_2 via the Krebs cycle, generating NADH and $FADH_2$, which are used by the electron transport chain (ETC) to pump protons toward the mitochondrial intermembrane space. This flux of protons builds the electromotive force that drives the production of ATP by oxidative phosphorylation (OxPhos). Additional OxPhos substrates include fatty acids, amino acids, and ketone bodies, all of which energize mitochondria via the ETC.

Lactate, which is made from pyruvate by the redox enzyme lactate dehydrogenase (LDH), serves to exchange carbons and energy between cells and tissues, moving via monocarboxylate transporters (MCTs[1–4]). Lactate is also an intercellular signal, acting through various mechanisms including redox ratio, G protein-coupled receptors, and post-translational modifications.[5–8]

In addition to these roles, lactate has been proposed to be directly oxidized by mitochondria, a model known as the intracellular lactate shuttle (ILS[9,10]). Despite receiving considerable experimental attention, ILS has remained controversial,[4,10] partly because of contrasting results and technical issues regarding the purity of subcellular fractions, the specificity of immunohistochemistry, and the poor retention of radiolabeled metabolites. Here, using genetically encoded fluorescent reporters, we find that mitochondria do not simply consume lactate; instead, energized mitochondria can produce and export lactate. This lactate vent offers a fast route to modulate matrix redox state and reactive oxygen species (ROS), reframing lactate as a mitochondrial stress-buffering output rather than only a metabolic fuel.

RESULTS

Most experiments were performed in HEK293 cells, a relatively oxidative epithelial cell line that is easy to handle. Other cell lines,

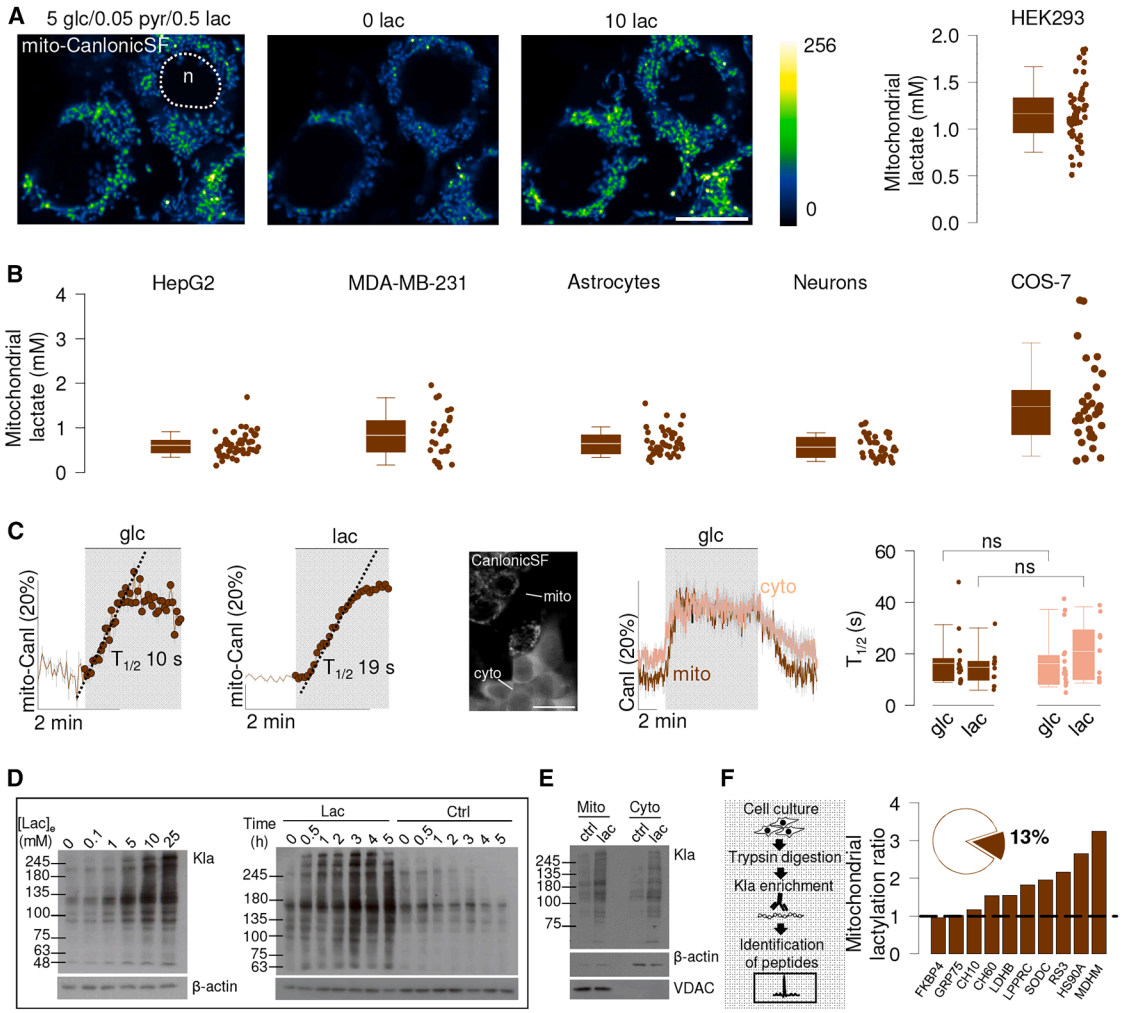

Figure 1. A dynamic mitochondrial lactate pool leads to protein lactylation

(A) HEK293 cells stably expressing mito-CanlonicSF (HEK040) were sequentially imaged at 5 mM glucose/0.05 mM pyruvate/0.5 mM lactate (standard buffer), 6 mM oxamate (nominal zero lactate) and high lactate (10 mM). Scale bar, 20 μm. Summary of lactate levels in standard buffer (five experiments, 53 cells). Location of a nucleus is indicated (n).

(B) The same protocol was applied to HepG2 (three experiments, 51 cells), MDA-MB-231 (three experiments, 26 cells), astrocytes (eleven experiments, 45 cells), neurons (eleven experiments, 19 cells), and Cos7 cells (six experiments, 32 cells). For brain cells, the standard buffer contained 2 mM glucose/0.05 mM pyruvate/0.5 mM lactate.

(C) Effect of glucose (5 mM) or lactate (10 mM) on HEK293 cells expressing mito-CanlonicSF or cytosolic CanlonicSF, measured simultaneously. Boxplot shows data from three experiments, 18 cells (Mann-Whitney, paired *t* test). Scale bar, 20 μm. NS, not significant.

(D) Lactate dose response and time response of whole-cell HEK293 protein lactylation (Kla antisera).

(E) Effect of lactate (25 mM/5 h) on protein lactylation (Kla antisera) of HEK293 subcellular fractions. Preparation purity was assessed by detection of VDAC (mitochondria) or β-actin (cytosol).

(F) Effect of lactate (25 mM/5 h) on the lactylation level of HEK293 mitochondrial proteins, identified by nano high-performance liquid chromatography-tandem mass spectrometry (nHPLC-MS/MS). Inset shows that 13% of precipitated proteins were mitochondrial. NS, not significant.

brain cells in culture, and neurons *in vivo* were studied to ascertain the general applicability and physiological relevance of the findings.

A dynamic lactate pool within mitochondria

According to the ILS hypothesis, there is lactate within mitochondria. In order to look for it, the single-fluorophore lactate indicator CanlonicSF[11] was stably expressed in HEK293 cells (HEK040 cell line). In the presence of physiological substrates, a steady-state pool of 1.2 mM lactate was found within the mitochondrial matrix (Figures 1A and S1). Determined in other cell types, mitochondrial lactate levels ranged between 0.6 and 1.5 mM (Figure 1B), suggesting that the pool is conserved. In response to extracellular glucose or lactate, mitochondrial lactate increased in the order of seconds (Figure 1C). Cytosolic and mitochondrial lactate moved in register, indicating that the permeability of the mitochondrial membrane is of the same order of magnitude as that of the plasma membrane. Lactate regulates histones and other proteins by a post-translational modification termed lactylation.[7,12] Figures 1D and S2 show that lactate

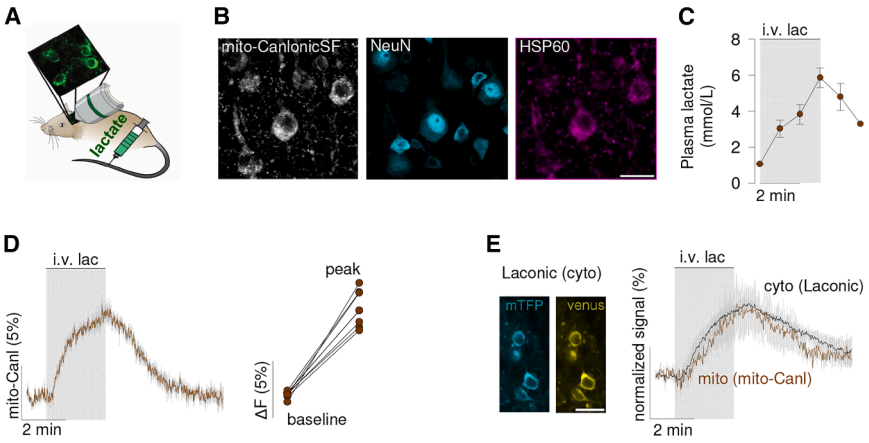

Figure 2. Mitochondrial lactate in neurons covaries with plasma lactate

(A) Mice expressing mito-CanlonicSF in neurons were i.v. injected with lactate (1.5 mmol/kg bodyweight).

(B) Colocalization of mito-CanlonicSF with the neuronal marker NeuN and the mitochondrial marker HSP60. Scale bar, 20 μm.

(C) Blood plasma lactate measurements upon lactate injection (data from three experiments in two animals).

(D) Mito-CanlonicSF response upon lactate injection (data from eight experiments in four animals).

(E) Paired measurement of lactate in mitochondria and cytosol, with mito-CanlonicSF and Laconic, respectively (normalized to peak, data from three experiments in three animals). Scale bar, 20 μm.

exposure led to widespread lactylation of HEK293 proteins in a dose- and time-dependent fashion. Several mitochondrial proteins became modified, including malate dehydrogenase (MDHM), lactate dehydrogenase B (LDHB), and superoxide dismutase (SODC; Figures 1E and 1F; Table S1). These modifications are of potential functional interest, as MDHM is part of the malate aspartate shuttle (MAS), and LDH and SODC are involved in hypoxia (see below).

To look for the mitochondrial lactate pool *in vivo*, mito-CanlonicSF was targeted to mouse somatosensory cortex neurons and imaged by two-photon microscopy (Figures 2A and 2B). An intravenous bolus injection of lactate led to a rise in blood lactate that peaked at 6 mM (Figure 2C), a level similar to that reported in exercising human subjects.[13] As shown in Figures 2D and 2E, this perturbation caused a rise in mitochondrial lactate that closely followed cytosolic lactate, as detected by Laconic.[14,15] Thus, the lactate pool of neuronal mitochondria is sensitive to physiological fluctuations in blood lactate.

Mitochondria transport lactate

Direct access to mitochondria was achieved by permeabilizing the plasma membrane (Figure 3A), a treatment that preserves mitochondrial respiration.[8,16] The permeabilization process was monitored by the release of cytosolic dyes and proteins (Figure S3). Integrity of the outer mitochondrial membrane was corroborated by retention of a fluorescent protein targeted to the intermembrane space (Figure S3), and by a functional ETC (see below), which requires retention of cytochrome *c* in the intermembrane space. In intact cells, exposure to pyruvate led to mitochondrial matrix acidification (Figure S3), which was attributed to MCT-mediated cytosolic acidification (Figure S3).[17] In contrast, in permeabilized cells, exposure to pyruvate led to mitochondrial matrix alkalinization caused by ETC activity (see below). This response to pyruvate was exploited as a routine demonstration of the quality of the preparation. No mitochondrial lactate increase was observed in response to glucose (Figure S3), confirming that glycolysis is disabled by the permeabilization procedure.

The uptake of lactate by mitochondria was saturable, displayed a Michaelis-Menten constant K_M of 0.8 mM (Figure 3B), and caused matrix acidification (Figure 3C). The non-metabolized pyruvate analog oxamate was able to elicit the phenomenon of trans-acceleration, characterized by lactate depletion followed by an overshoot upon substrate removal (Figure 3D). The phenomenon of trans-acceleration, or accelerated exchange, is a signature of carrier-mediated transport, where the translocation of a substrate in one direction makes it more probable that a second substrate moves in the opposite direction by increasing the number of available empty transport sites on the other side of the membrane. At physiological concentrations, pyruvate also trans-accelerated lactate, showing that the mitochondrial lactate transport system carries pyruvate as well. Surprisingly, at higher pyruvate concentrations, the depletion of lactate turned into accumulation in some experiments (Figure 3E). Production of lactate from pyruvate pointed to LDH activity, a key observation that was pursued below.

The possibility that MCTs are involved in mitochondrial lactate transport was approached by pharmacological means. The potent MCT1 and MCT2 blocker AR-C155858,[18] which inhibits surface monocarboxylate uptake in HEK293 cells by >95%,[15,19,20] was a weak inhibitor of mitochondrial lactate uptake (Figure 3F). AZD3965, another MCT1/MCT2 blocker,[21] was also relatively ineffective. pCMBS, a blocker of MCT1 and MCT4, but not of MCT2,[22] inhibited mitochondrial lactate uptake by about 50% (Figure 3F). To our surprise, the most effective inhibitor of mitochondrial lactate uptake was UK5099 (Figure 3F), considered a specific blocker of the mitochondrial pyruvate carrier (MPC).[22–24] When lactate uptake was probed in the presence of a cocktail containing AR-C155858, pCMBS, syrosingopine (MCT1/4 inhibitor), and UK5099, the inhibition was not stronger than that obtained with UK5099 alone. In short, the functional and pharmacological profiles of mitochondrial lactate transport do not match those of typical plasma membrane MCTs. In view of the effectiveness of UK5099, we probed cells devoid of MPC2 using CRISPR.[25] MPC2 gene deletion, which abrogated the uptake of pyruvate, reduced the uptake of lactate by about 50% (Figures 3G, 3H, and S4). These pharmacological and genetic interventions converge to indicate that the MPC participates in the transport of lactate. An in-depth characterization of lactate transport by the MPC has been presented elsewhere.[26] Of note, MPC deletion eliminated the production of lactate from pyruvate in permeabilized cells, providing

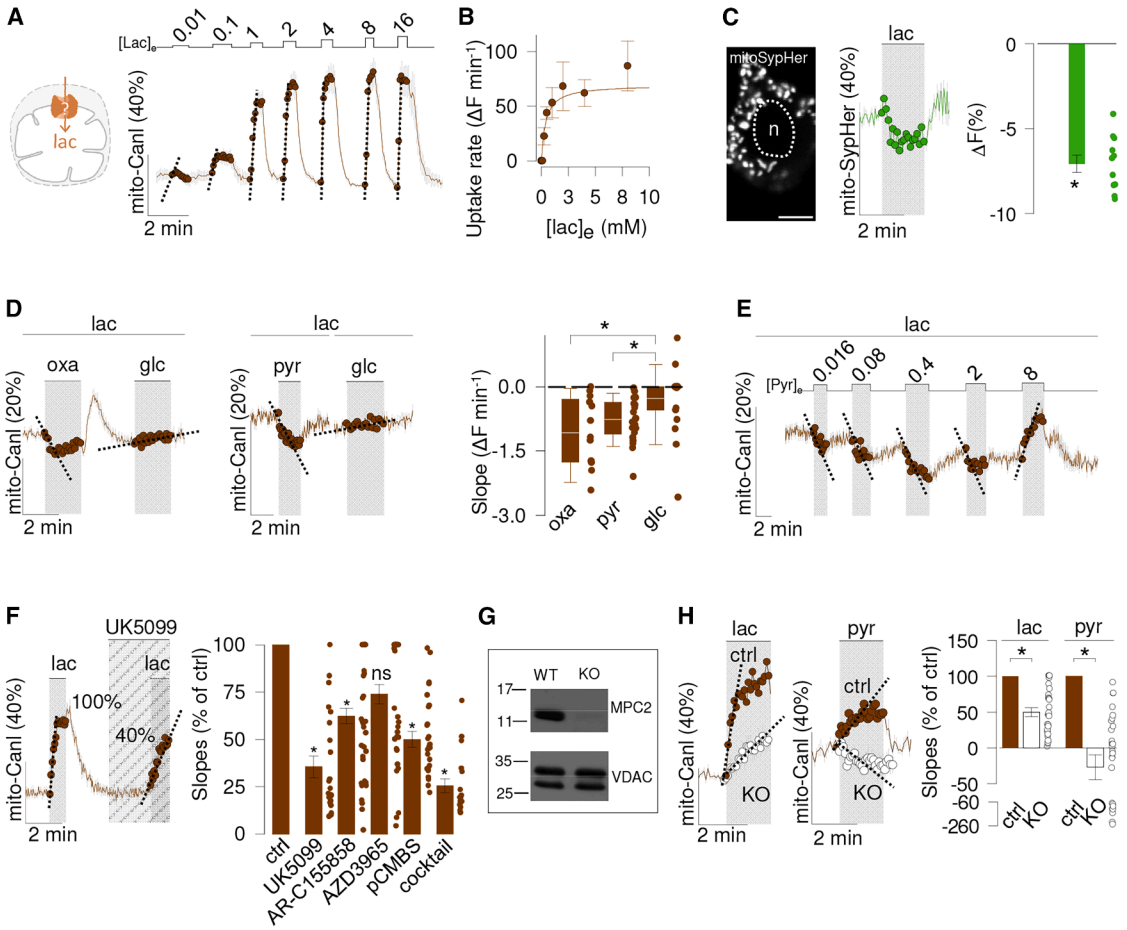

Figure 3. Characterization of mitochondrial lactate transport

Direct access of lactate to mitochondria was obtained by permeabilizing HEK293 cells with digitonin. Except for the lactate dose-response curve, mitochondria were kept energized with 0.2 mM glutamate plus 0.1 mM malate.

(A) Dose response of lactate uptake (mM) in cells expressing mito-CanlonicSF.

(B) A rectangular hyperbola was fitted to the initial uptake rates giving a K_M = 0.8 ± 0.3 (four experiments, 75 cells).

(C) Cells expressing the pH sensor mito-SypHer. The nucleus is indicated (*n*). Scale bar, 20 μm. Effect of 2 mM lactate on matrix pH. Bar graph summarizes data from two experiments (16 cells).

(D) Mitochondria perfused with 0.5 mM lactate were exposed to oxamate (6 mM), pyruvate (0.5 mM), and glucose (5 mM). Initial slopes of lactate depletion are shown and are summarized in the bar graph (two experiments, 13 cells, paired *t* test).

(E) Mitochondria perfused with 0.5 mM lactate were exposed to increasing concentrations of pyruvate (mM; representative of two experiments, 19 cells).

(F) Lactate uptake was measured in the absence and presence of UK5099 (0.5 μM). Bar graph summarizes data from similar experiments with a panel of inhibitors. Ctrl (DMSO 0.01%–0.05%; nine experiments, 57 cells); UK5099 (0.5 μM; four experiments, 23 cells); AR-C155858 (1 μM; five experiments, 38 cells); AZD3965 (10 μM; five experiments, 36 cells); pCMBS (50 μM; four experiments, 25 cells); inhibitor cocktail contains UK5099, AR-C155858, pCMBS, and 5 μM syrosingopine (three experiments, 18 cells). Paired *t* test.

(G) MPC2 expression in wild-type (WT) and CRISPR-edited HEK293 cells (sgMPC2KO7). Representative of three experiments. Molecular weights (kDa) are indicated.

(H) MPC2KO and control cells were exposed to lactate (10 mM) and pyruvate (10 mM). Bar graph summarizes three knockout (KO) experiments (27 cells) and three controls (40 cells). Unpaired *t* test. *$p < 0.05$. Data are presented as individual cells (mean ± SEM).

independent support to the presence of LDH activity within the mitochondrial matrix.

Mitochondria are not energized by lactate

With evidence of inner-membrane lactate transport and matrix LDH activity, the two pillars of ILS, we first sought proof of effective lactate metabolism by measuring autofluorescence, which reports the redox status of mitochondria. At 360 nm excitation, autofluorescence is proportional to the combined NADH and NADPH pools, while at 488 nm excitation, emission reflects FAD^+ and flavoproteins.[27–29] As expected, application of pyruvate that had been pre-incubated with glutamate/malate caused reciprocal changes in NAD(P)H and FAD^+/flavoprotein autofluorescence (Figures 4A and 4B). However, lactate was without effect. Autofluorescence has specificity limitations, is chiefly ascribed to protein-bound cofactors, and it may fail to detect flux if PDH/Krebs cycle production was matched by ETC consumption. Thus, we imaged the activity of the ETC by monitoring

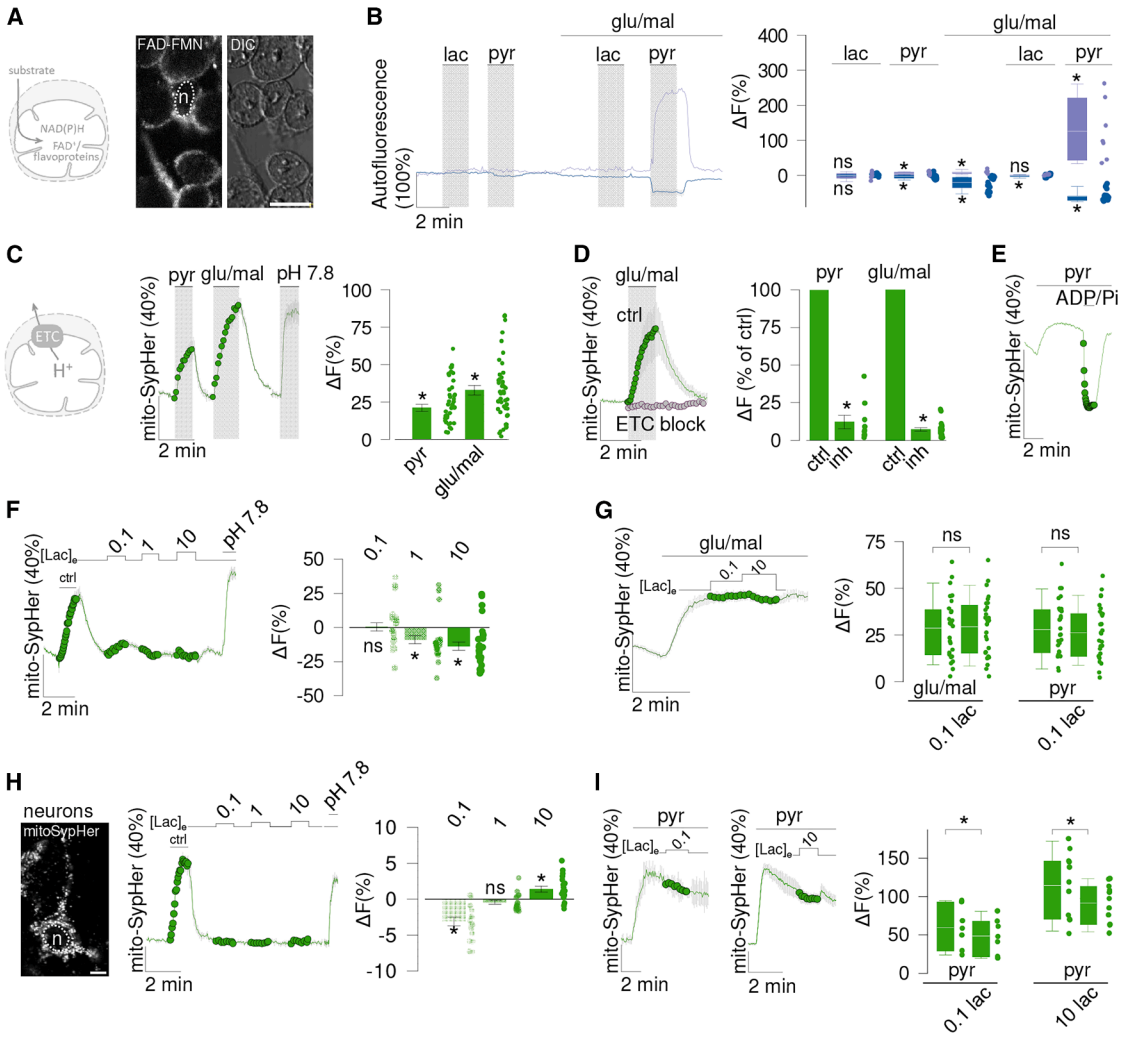

Figure 4. Mitochondrial energization is not supported by lactate

HEK293 cells were permeabilized with digitonin and exposed to 0.1 mM pyruvate (pyr), 0.1 mM lactate (lac), 0.2 mM glutamate (glu), or 0.1 mM malate (mal).

(A) NAD(P)H and FAD^+/flavoprotein can be detected as autofluorescence. Right: FAD^+/flavoprotein autofluorescence and corresponding DIC image. A nucleus is indicated (*n*). Scale bar, 20 μm.

(B) Effect of substrates on NAD(P)H (magenta) and FAD^+/flavoprotein autofluorescence (blue). Bar graph shows the summary of five experiments each for NAD(P)H (50 cells, 10 cells per region of interest [ROI]; paired *t* test) and FAD^+/flavoprotein (28 cells; Wilcoxon signed-rank test).

(C) The ETC alkalinizes the matrix by pumping protons. Right: matrix alkalinization was assessed with mito-SypHer after addition of pyr, glu/mal, or pH 7.8-adjusted buffer. Bar graph summarizes the maximum change (nine experiments, 47 cells).

(D) Mitochondria were exposed to glu/mal in the presence of ETC inhibitors (rotenone, 1 μM; antimycin, 1 μM). Bar graph summarizes data for pyr (three experiments, 9 cells) and glu/mal (five experiments, 20 cells).

(E) Pyruvate-energized mitochondria were exposed to ADP (2 mM) and Pi (2 mM) (three experiments, 21 cells).

(F) After a control (ctrl) pulse of glu/mal, mitochondria were exposed to increasing concentrations of lactate (mM). Bar graph shows change relative to baseline (six experiments, 28 cells).

(G) Glu/mal-energized mitochondria were exposed to 0.1 or 10 mM lactate. Summary of five experiments (28 cells).

(H) A neuron expressing mito-SypHer, with the nucleus indicated (*n*). Scale bar, 10 μm. After a control pulse of pyruvate (ctrl), neurons were exposed to increasing concentrations of lactate (mM). Summary of data (four experiments, 18 cells).

(I) In the presence of pyruvate, mitochondria in neurons were exposed to 0.1 or 10 mM lactate. Summary of data (five experiments, 21 cells). Paired *t* test. NS, not significant; $*p < 0.05$.

changes in matrix pH in response to oxidizable substrates (Figure 4C).[29] Indeed, addition of pyruvate or mimicking the mitochondrial phase of the MAS with glutamate/malate elicited a rapid rise in matrix pH, which was precluded by pharmacological ETC inhibition (Figures 4C and 4D). As expected, the alkalinization by pyruvate was partially reverted by activation of the F_1F_o-ATPase with ADP and inorganic phosphate (Figure 4E). These results confirm that the pH change induced by substrates reflects the pumping of protons by the ETC. Notably, the entry of protons via the MPC, one per pyruvate, is negligible compared

with the 30 protons that are extruded by the ETC for every pyruvate that is metabolized to CO_2.[29] Next, we tested the ability of lactate to drive the ETC. Lactate had no detectable impact on matrix pH in HEK293 cells, either de-energized or energized (Figures 4F and 4G). Neuronal mitochondria also showed a robust ETC-mediated matrix alkalinization by pyruvate, but not at all by lactate (Figures 4H and 4I).

Mitochondrial lactate production modulates H_2O_2 matrix level

Having failed to detect lactate metabolism by mitochondria, experiments were designed to test for lactate production. First, a 10-cm dish of permeabilized HEK293 cells treated for 1 h with pyruvate, malate, and glutamate was found to raise extracellular lactate by 280 μM (Table S2). Further to discern the subcellular source, we studied mitochondria isolated by differential centrifugation. Here, the mitochondrial fraction harvested from three 10-cm dishes and incubated for 1 h with pyruvate, malate, glutamate, and lactate, all at 0.5 mM, was able to elevate extracellular lactate from 478 to 845 μM (Table S3). To investigate short-term lactate production dynamics, we engineered eLiLac, an outward-facing plasma membrane sensor made by cloning an Igκ leader sequence to the N terminus and a GPI anchor to the C terminus of the lactate sensor LiLac,[30] as was previously reported for the iGluSnFR glutamate sensor.[31] As predicted by mitochondrial lactate production, pyruvate superfusion of permeabilized neurons that had been pre-energized with glutamate/malate led to a dose-dependent increase in eLiLac signal (Figure 5A). Note that the LiLac scaffold is insensitive to pyruvate in the mM range.[30] A fourth line of evidence was obtained with a transport-stop protocol in cells expressing mito-CanlonicSF. Acute pharmacological inhibition of the MPC in energized mitochondria led to accumulation of matrix lactate (Figure 5B, right). Control experiments showed that CanlonicSF is insensitive to glutamate and malate but displays a small response to millimolar pyruvate (Figure S1). However, the latter cannot explain the observed effect, for UK5099 decreases matrix pyruvate (Figure S5). Note that because MPC blockage by UK5099 is partial,[32] there is plenty of pyruvate left in the matrix to sustain PDH, whose affinity for pyruvate lies in the low micromolar range. No lactate accumulation was observed upon MPC blockage in cells incubated solely with pyruvate or solely with glutamate/malate (Figure S5). Fully energized mitochondria failed to accumulate lactate in response to AR-C155858 (Figure S5), indicating that MCT1 and MCT2 are not involved in lactate extrusion. Altogether, these experiments in permeabilized cells and isolated mitochondria show that mitochondria are lactate producers.

A major factor for the production of ROS is the ratio between NADH and NAD^+ in the mitochondrial matrix.[33] Considering that for every lactate generated from pyruvate, one NADH is converted into NAD^+, we tested whether the release of lactate might have an impact on the production of ROS. To this aim, the choice H_2O_2 sensor HyPer7.2[34,35] was expressed in the mitochondrial matrix of HEK293 cells, which were permeabilized. In order to work within the optimum detection range of the sensor, mitochondria were treated with the GSH-oxidizing agent diamide. Figure 5C shows that under these conditions, HyPer7.2 was able to respond to the addition of nM H_2O_2, approaching physiological level guidelines.[35] Addition of the MPC blocker led to a quick rise in endogenous H_2O_2 (Figure 5D). By impairing the acceptance of electrons at complex IV, hypoxia jams the ETC, leading to the accumulation of NADH.[33] Strikingly, lowering oxygen from 230 to 62 μM,[36,37] a mild hypoxia, caused a further, reversible increase in H_2O_2, which was not apparent in the absence of the MPC blocker (Figure 5E). While correlative, these results are consistent with a mechanism in which the release of lactate via the MPC serves to reduce the production of ROS, a kind of energy and redox vent. Consistent with this model, hypoxia reversibly stimulated the production of lactate by mitochondria (Figure 5F). We do not know whether this level of hypoxia is capable of stimulating glycolysis. In summary, we claim that mitochondria produce lactate when NADH in the matrix is high and that the release of lactate via the MPC ameliorates the production of ROS (Figure 5G).

DISCUSSION

We looked for lactate consumption by mitochondria but found instead that they are lactate producers and that the release of lactate modulates ROS levels. These conclusions are based on the following observations: (1) a dynamic lactate pool in the matrix, (2) a high-affinity lactate transport system in the inner membrane, (3) MPC-sensitive lactate production from pyruvate, (4) redox-sensitive lactate production from pyruvate, (5) stimulation of lactate production by hypoxia, (6) increased matrix lactate and H_2O_2 levels in response to MPC inhibition, and (7) accumulation of lactate and H_2O_2 by hypoxia under MPC inhibition. In addition, we observed that lactate induces the lactylation of mitochondrial proteins and that lactate in neuronal mitochondria covaries with blood lactate.

ILS hypothesis

The original ILS hypothesis stated that lactate is transported into the mitochondrial matrix and then metabolized to pyruvate to sustain respiration. Evidence supporting ILS included immunohistochemical detection of MCTs, LDH, and CD147; monitoring of added NADH; and respirometry of purified mitochondria.[4,10] Some issues regarding ILS include antibody specificity and possible contamination of mitochondrial preparations with cytosolic enzymes.[4,38] The revised, more eclectic version of ILS has LDH in the intermembrane space,[10,39] which is topologically equivalent to the cytosol, but the debate is still ongoing. Two studies reported that purified mitochondria consumed oxygen in the presence of lactate,[40,41] whereas a more recent one showed that the addition of isotopically labeled lactate to purified mitochondria did not result in Krebs cycle labeling unless exogenous LDHA was expressed in the organelle.[8] Interestingly, lactate was found to stimulate respiration directly, independent of its metabolism, which may help to explain some of the previous conflicting results. By showing that lactate does not energize mitochondria our results align with the latter study.

Lactate and pyruvate transport

Mitochondrial lactate responded to changes in extracellular lactate. It is not possible at this stage to differentiate between lactate entry, decreased lactate efflux, or increased lactate production. We would like to argue that the accumulation in the

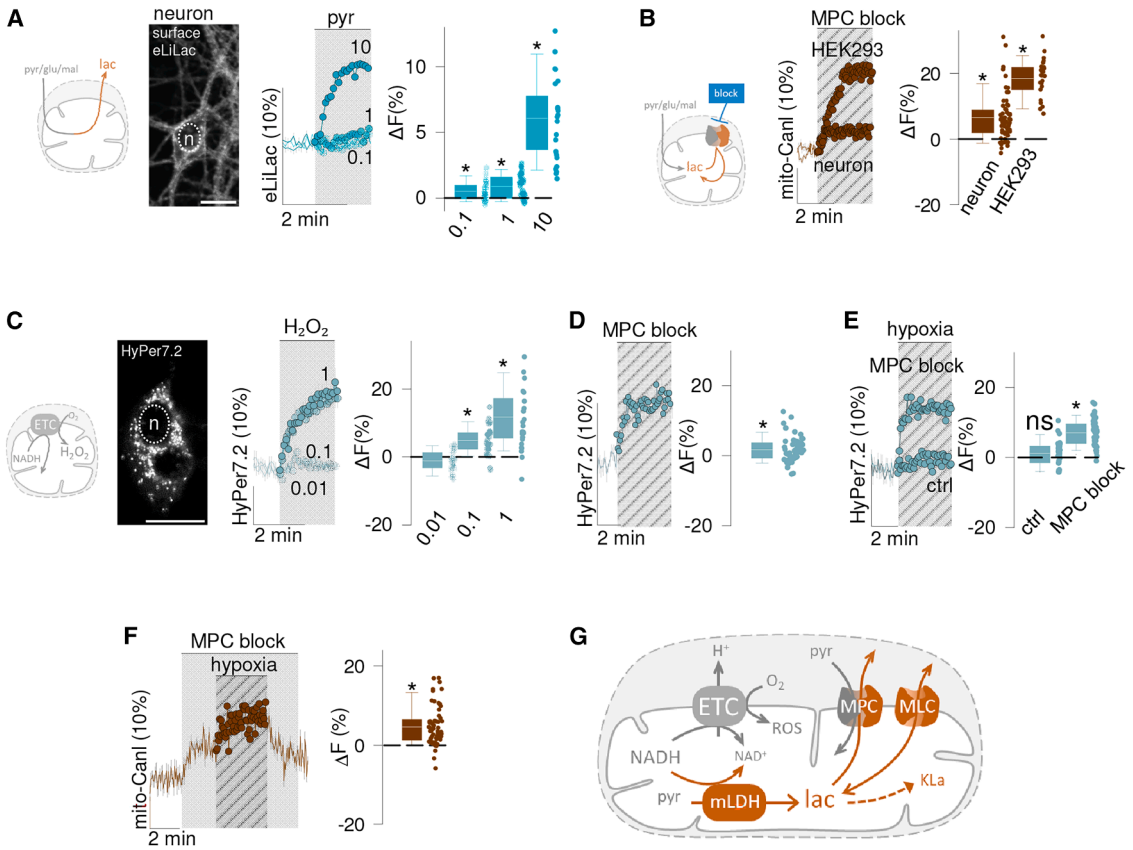

Figure 5. Mitochondrial lactate flux modulates redox homeostasis

Experiments were conducted in digitonin-permeabilized HEK293 cells and neurons.

(A) Extracellular lactate detected with eLiLac in permeabilized neurons at increasing concentrations of pyruvate (mM). The nucleus is indicated (*n*). Scale bar, 20 μm. Perfusates contained 0.2 mM glutamate and 0.1 mM malate. Summary of data from four experiments (36 cells).

(B) Mitochondrial lactate was assessed using mito-CanlonicSF. The effect of MPC inhibition by 1 μM UK5099 was evaluated under 10 mM pyruvate/0.2 mM glutamate/0.1 mM malate/0.5 mM lactate. Data are from four experiments in HEK293 cells (24 cells) and nine in neurons (65 cells).

(C) Mitochondrial hydrogen peroxide (H_2O_2) levels as a readout of ROS production were measured using matrix-targeted HyPer7.2 in HEK293 cells. The nucleus is indicated (*n*). Scale bar, 20 μm. Mitochondria were exposed to increasing H_2O_2 (μM) in the presence of 0.1 mM pyruvate/0.2 mM glutamate/0.1 mM malate/0.01 mM diamide. Summary of three experiments (30 cells).

(D) H_2O_2 accumulation in response to 1 μM UK5099 was evaluated under 10 mM pyruvate/0.2 mM glutamate/0.1 mM malate/0.5 mM lactate, and 0.01 mM diamide. Data from four experiments (49 cells).

(E) Effect of acute hypoxia (N_2 gassing) on H_2O_2 levels in same conditions as (D) with/without MPC block with 1 μM UK5099. Ctrl (0.01% DMSO; three experiments, 30 cells) and UK5099-treated (five experiments, 49 cells).

(F) In neurons, UK5099 inhibition promotes mitochondrial lactate accumulation under same conditions as (B) and (D). Summary of seven experiments (60 cells). Paired *t* test; $^*p < 0.05$.

(G) Proposed model: at high NADH, electrons may produce ROS at the ETC or funneled into lactate, which leaves mitochondria via the MPC. The MLC allows parallel movement of lactate. Mitochondrial lactate promotes lysine lactylation of matrix proteins (Kla).

matrix does not result from pyruvate uptake followed by pyruvate-to-lactate conversion for the following reasons: (1) pyruvate was very efficient at energizing mitochondria. Therefore, if some pyruvate had entered the matrix, either generated from lactate or as a contaminant in the lactate stock, it would have shown as matrix alkalization, which was not observed. (2) Figure 3H shows that the generation of lactate from pyruvate within the matrix was fully blocked by MPC deletion. However, lactate accumulation in response to lactate exposure was inhibited by only 50%. This means that there is a lactate entry pathway that is independent of pyruvate entry. (3) Lactate accumulation was sensitive to AR-C155858, which is not known to affect the MPC. (4) Regarding the accumulation of matrix lactate *in vivo*, it may not be explained by increased cytosolic pyruvate because cytosolic pyruvate actually goes down, secondary to trans-acceleration at surface MCTs.[14]

The saturable nature, an affinity in the low millimolar range, and the possible ability to carry protons, pyruvate, and oxamate first pointed to an MCT. Acidification is suggestive but not definitive proof of proton co-transport, as the possibility remains that it reflects LDH working in the reverse mode (or other dehydrogenases; see below). In view of the observed inability of lactate to affect autofluorescence or energize the ETC, we do not favor the possibility of lactate metabolism. However, an unambiguous demonstration of proton co-transport must wait for a more controlled experimental design without confounding metabolic activity. Previously,

antibodies against MCT1 and MCT2 had detected epitopes associated with mitochondria[9,42] and lower mitochondrial lactate was reported in skeletal muscle genetically depleted of MCT1.[43] However, we do not favor MCT1 involvement, at least in HEK293 cells. At 0.8 mM, the K_M of lactate uptake lies in the range of MCT2 (0.5–0.75 mM) and MCT4 (0.7–1 mM) and is lower than that reported for MCT1 (3.5–10 mM[19,22]). The weak inhibitory effects of the MCT1/2 inhibitors AR-C155858 and AZD3965 speak against a mandatory role for these isoforms. Syrosingopine and pCMBS, which block MCT1 and MCT4, but not MCT2, also achieved partial inhibition. The best effect was achieved with the MPC blocker UK5099, whereas genetic deletion of the MPC reduced lactate uptake by about 50%. Because of the standing inward pyruvate gradient[32] and the effective trans-acceleration of lactate by pyruvate, we surmise that the MPC is better poised to work as a lactate extruder (Figure 5F). According to the literature, lactate is not a substrate of the MPC, a notion that may be traced back to the seminal study by Andrew Halestrap, who, along with the introduction of UK5099 and other major advances, observed that lactate did not transaccelerate the efflux of radiolabeled pyruvate from isolated mitochondria.[44] We have submitted a preprint that demonstrates MPC-mediated lactate transport,[26] which is not in conflict with the data in Halestrap.[44] In view of the unusual functional/pharmacological profile, the remaining lactate permeability may not be ascribed to a specific MCT isoform. Its molecular identification may not be straightforward, as genetic deletion of metabolite transporters may lead to unexpected compensatory changes.[45] Meanwhile, we propose the operational term mitochondrial lactate carrier (MLC; Figure 5G).

Roles of mitochondrial lactate

To the best of our understanding, mammalian cells have no enzyme other than LDH capable of converting pyruvate to lactate in a redox-sensitive manner. However, mitochondrial dehydrogenases have been shown to be promiscuous.[46] With that caveat, we argue here for a functional module consisting of matrix LDH and MPC/MLC, which plays the role of de-energizing the mitochondria. The concentration of pyruvate and the NADH/NAD^+ ratio in the matrix have been recently determined, enabling a thermodynamic analysis. The net direction of the LDH reaction is governed by its equilibrium constant and the concentrations of pyruvate, lactate, NADH, NAD^+, and H^+. With the equilibrium constant (K_{eq}) of 1.11×10^{-11} M and an NADH/NAD^+ ratio of 0.125,[47] pH at 7.8,[48] and matrix pyruvate at 30 μM,[32] mitochondria should be able to push lactate up to 68 mM, almost two orders of magnitude higher than that observed by us and others.[49] This means that under physiological conditions, mitochondrial LDH works far from equilibrium and in the direct mode (pyruvate to lactate), which explains the failure of lactate to energize the ETC, at the non-physiological low NADH/NAD^+ ratio of 0.009.[50] Low mitochondrial LDH activity may explain the difficulty of isolating the enzyme against the background of the very abundant cytosolic LDH. Its running in the direct mode is consistent with the recent observation in purified mitochondria that radiolabeled lactate was not incorporated into TCA cycle intermediates unless LDHA was targeted to the matrix,[8] an intervention bound to dissipate the redox potential of the organelle.[4] Mitochondrial lactate consumption could in principle proceed when matrix pyruvate and NADH/NAD^+ are very low while lactate is very high, perhaps in exercising muscle fibers,[51] a possibility now open to experimental testing.

Our results show that under substrate conditions prevailing in healthy cells, mitochondrial LDH runs in the direct mode, slowly converting NADH into NAD^+, so that electrons are passed to lactate, which then leaves the matrix and possibly the cell. What could be the point of such a continuous waste of energy and carbon? A key to this question is hypoxia. When oxygen is low, electrons pile up in the form of NADH. Cells are known to reduce such redox stress by expressing uncoupling proteins (UCPs) that shortcut the ETC, bringing down matrix NADH levels and the production of ROS.[37] To exert their protective role, UCPs use oxygen and dissipate the energy irreversibly, as heat. The lactate vent is faster, does not require oxygen, and saves energy as a transient lactate pool that may be shifted within the tissue and beyond. In brain tissue, lactate diffuses away from the active zone and engages G protein-coupled receptors and other targets for the inhibition of neural activity and energy metabolism, promoting scale-spanning coordination between short-ranged metabolism and long-ranged information processing.[52]

LDH is highly regulated, and its partial pharmacological inhibition has consequences,[53,54] observations that have been puzzling because neither regulation nor partial inhibition should affect flux in a near-equilibrium reaction. In contrast, our data suggest that mitochondrial LDH works far from equilibrium. Now that a functional assay specific for mitochondrial LDH is available, it will be easier to investigate its biology and regulation, for example, by lactylation. Lactate can stimulate the ETC directly, acting as a signal independently of its metabolism.[8] The ability of mitochondria to generate their own lactate suggests a possible mechanism for the control of respiration and/or ROS production in subcellular domains. Other pending questions pertain to the relationship between mitochondrial and cytosolic lactate production. Is mitochondrial lactate recycled locally in the cytosol, or is it instead released to the extracellular space to be recycled by other cells or tissues? Given the abundance of LDH in the cytosol and the smaller volume fraction of mitochondria, we do not expect mitochondria to match glycolysis in terms of maximum lactate production rate, but conceivably, mitochondria may be more sensitive to hypoxia and other stressors than glycolysis.

Limitations of the study

Lactate has been found in the mitochondrial matrix of every mammalian cell investigated so far, by us and others, both *in vitro* and *in vivo*, but our claim regarding lactate production and its link to ROS production is based on data collected solely from HEK293 cells and neurons cultured *in vitro*. The conditions, physiological and pathophysiological, under which the energy vent becomes relevant *in vivo* remain to be established. Another caveat regards universality. Even within a given cell, mitochondria differ greatly in terms of size, shape, relationship with other organelles, Ca^{2+} handling, DNA dosage, etc. They are also bound to be heterogeneous in terms of OxPhos and energy venting.

RESOURCE AVAILABILITY

Lead contact

Requests for further information and resources should be directed to and will be fulfilled by the lead contact, L. Felipe Barros, luis.barros@uss.cl.

Materials availability

All unique/stable reagents generated in this study are available from the lead contact with a completed materials transfer agreement.

Data and code availability

- Unprocessed data underlying the display items in the manuscript, related to Figures 1, 2, 3, 4, 5, and S1–S5, and uncropped western blots are available in Data S1. Data have been deposited to Mendeley Data at 10.17632/3jcp9t922s.2 and are publicly available as of the date of publication.
- This paper does not report original code.
- Any additional information required to reanalyze the data reported in this paper is available from the lead contact upon request.

ACKNOWLEDGMENTS

We thank an anonymous reviewer for suggesting the term "vent." We thank Karen Everett for critical reading of the manuscript and members of the Energy Metabolism Group at CECs for helpful discussions. We thank Jason Cantor and Gary Yellen for sharing plasmids. This work was funded partly by Fondecyt projects 1230145 (to L.F.B.), 11190678 (to I.R.), and 1230682 (to I.R.); NIH R01 NS126920-01A1 (Phil O'Herron, PI; L.F.B., co-I); and Proyecto USS-FIN-23-FAPE-03 (to P.Y.S.). We also thank Fondequip EQM190142 (to C.A.-N.) and Fondequip EQY24004 (to L.F.B.).

AUTHOR CONTRIBUTIONS

Conceptualization, D.R. and L.F.B.; methodology, D.R., Y.C.-B., J.D., L.R., M.T.W., C.A.-N., A.S.M., B.W., P.Y.S., and L.F.B.; formal analysis, D.R., Y.C.-B., A.J.G., S.H.-G., H.F., N.C.-L., R.S., A.v.F.-C., F.S., V.M.-G., F.B.-L., I.R., M.T.W., C.A.-N., P.Y.S., and L.F.B.; investigation, D.R., Y.C.-B., A.J.G., S.H.-G., H.F., N.C.-L., R.S., J.L.A., A.v.F.-C., F.S., V.M.-G., F.B.-L., and P.Y.S.; writing – original draft, D.R. and L.F.B.; writing – review and editing, D.R., Y.C.-B., A.J.G., S.H.-G., H.F., N.C.-L., R.S., A.v.F.-C., F.S., V.M.-G., J.D., L.R., M.T.W., F.B.-L., I.R., C.A.-N., A.S.M., B.W., P.Y.S., and L.F.B.; visualization, D.R., A.v.F.-C., M.T.W., C.A.-N., P.Y.S., and L.F.B.; supervision, M.T.W., I.R., C.A.-N., A.S.M., B.W., P.Y.S., and L.F.B.; project administration, L.F.B.; funding acquisition, I.R., C.A.-N., B.W., P.Y.S., and L.F.B.

DECLARATION OF INTERESTS

The authors declare no competing interests.

STAR★METHODS

Detailed methods are provided in the online version of this paper and include the following:

- KEY RESOURCES TABLE
- EXPERIMENTAL MODEL AND STUDY PARTICIPANT DETAILS
  - Animals
  - Cell lines
- METHOD DETAILS
  - Culture of cell lines
  - Reporter cell lines and MPC2KO
  - Neural cultures
  - In vivo assays
  - Transfection/infection for in vitro sensor expression
  - Immunohistochemistry
  - Fluorescent dye loading
  - In vitro imaging
  - Calibration of mito-CanIonicSF
  - Extracellular lactate determination
  - Mitochondrial isolation
  - Lactate determination in the supernatant of isolated mitochondria
  - Lactylation analysis
- QUANTIFICATION AND STATISTICAL ANALYSIS

SUPPLEMENTAL INFORMATION

Supplemental information can be found online at https://doi.org/10.1016/j.cmet.2026.02.020.

Received: December 5, 2024
Revised: August 10, 2025
Accepted: February 26, 2026
Published: March 24, 2026

REFERENCES

1. Cori, C.F., and Cori, G.T. (1929). Glycogen formation in the liver from d- and l-lactic acid. Biol. Chem. *81*, 389–403. https://doi.org/10.1016/S0021-9258(18)83822-4.
2. Pellerin, L., and Magistretti, P.J. (1994). Glutamate uptake into astrocytes stimulates aerobic glycolysis: a mechanism coupling neuronal activity to glucose utilization. Proc. Natl. Acad. Sci. USA *91*, 10625–10629. https://doi.org/10.1073/pnas.91.22.10625.
3. Hui, S., Ghergurovich, J.M., Morscher, R.J., Jang, C., Teng, X., Lu, W., Esparza, L.A., Reya, T., Le, Z., Yanxiang Guo, J., et al. (2017). Glucose feeds the TCA cycle via circulating lactate. Nature *551*, 115–118. https://doi.org/10.1038/nature24057.
4. Glancy, B., Kane, D.A., Kavazis, A.N., Goodwin, M.L., Willis, W.T., and Gladden, L.B. (2021). Mitochondrial lactate metabolism: history and implications for exercise and disease. J. Physiol. *599*, 863–888. https://doi.org/10.1113/JP278930.
5. Ahmed, K., Tunaru, S., Tang, C., Müller, M., Gille, A., Sassmann, A., Hanson, J., and Offermanns, S. (2010). An autocrine lactate loop mediates insulin-dependent inhibition of lipolysis through GPR81. Cell Metab. *11*, 311–319. https://doi.org/10.1016/j.cmet.2010.02.012.
6. Barros, L.F. (2013). Metabolic signaling by lactate in the brain. Trends Neurosci. *36*, 396–404. https://doi.org/10.1016/j.tins.2013.04.002.
7. Zhang, D., Tang, Z., Huang, H., Zhou, G., Cui, C., Weng, Y., Liu, W., Kim, S., Lee, S., Perez-Neut, M., et al. (2019). Metabolic regulation of gene expression by histone lactylation. Nature *574*, 575–580. https://doi.org/10.1038/s41586-019-1678-1.
8. Cai, X., Ng, C.P., Jones, O., Fung, T.S., Ryu, K.W., Li, D., and Thompson, C.B. (2023). Lactate activates the mitochondrial electron transport chain independently of its metabolism. Mol. Cell *83*, 3904–3920.e7. https://doi.org/10.1016/j.molcel.2023.09.034.
9. Brooks, G.A., Dubouchaud, H., Brown, M., Sicurello, J.P., and Butz, C.E. (1999). Role of mitochondrial lactate dehydrogenase and lactate oxidation in the intracellular lactate shuttle. Proc. Natl. Acad. Sci. USA *96*, 1129–1134. https://doi.org/10.1073/pnas.96.3.1129.
10. Brooks, G.A. (2018). The science and translation of lactate shuttle theory. Cell Metab. *27*, 757–785. https://doi.org/10.1016/j.cmet.2018.03.008.
11. Aburto, C., Galaz, A., Bernier, A., Sandoval, P.Y., Holtheuer-Gallardo, S., Ruminot, I., Soto-Ojeda, I., Hertenstein, H., Schweizer, J.A., Schirmeier, S., et al. (2022). Single-fluorophore indicator to explore cellular and subcellular lactate dynamics. ACS Sens. *7*, 3278–3286. https://doi.org/10.1021/acssensors.2c00731.
12. Hagihara, H., Shoji, H., Otabi, H., Toyoda, A., Katoh, K., Namihira, M., and Miyakawa, T. (2021). Protein lactylation induced by neural excitation. Cell Rep. *37*, 109820. https://doi.org/10.1016/j.celrep.2021.109820.
13. Dalsgaard, M.K. (2006). Fuelling cerebral activity in exercising man. J. Cereb. Blood Flow Metab. *26*, 731–750. https://doi.org/10.1038/sj.jcbfm.9600256.
14. Mächler, P., Wyss, M.T., Elsayed, M., Stobart, J., Gutierrez, R., von Faber-Castell, A., Kaelin, V., Zuend, M., San Martín, A., Romero-Gómez, I., et al. (2016). In vivo evidence for a lactate gradient from astrocytes to neurons. Cell Metab. *23*, 94–102. https://doi.org/10.1016/j.cmet.2015.10.010.
15. San Martín, A., Ceballo, S., Ruminot, I., Lerchundi, R., Frommer, W.B., and Barros, L.F. (2013). A genetically encoded FRET lactate sensor and its use

to detect the Warburg effect in single cancer cells. PLoS One *8*, e57712. https://doi.org/10.1371/journal.pone.0057712.

16. Divakaruni, A.S., Rogers, G.W., and Murphy, A.N. (2014). Measuring mitochondrial function in permeabilized cells using the Seahorse XF Analyzer or a Clark-type oxygen electrode. Curr. Protoc. Toxicol. *60*, 25.2.1–25.216. https://doi.org/10.1002/0471140856.tx2502s60.
17. Azarias, G., Perreten, H., Lengacher, S., Poburko, D., Demaurex, N., Magistretti, P.J., and Chatton, J.Y. (2011). Glutamate transport decreases mitochondrial pH and modulates oxidative metabolism in astrocytes. J. Neurosci. *31*, 3550–3559. https://doi.org/10.1523/JNEUROSCI.4378-10.2011.
18. Ovens, M.J., Davies, A.J., Wilson, M.C., Murray, C.M., and Halestrap, A.P. (2010). AR-C155858 is a potent inhibitor of monocarboxylate transporters MCT1 and MCT2 that binds to an intracellular site involving transmembrane helices 7-10. Biochem.J. *425*, 523–530. https://doi.org/10.1042/BJ20091515.
19. Contreras-Baeza, Y., Sandoval, P.Y., Alarcón, R., Galaz, A., Cortés-Molina, F., Alegría, K., Baeza-Lehnert, F., Arce-Molina, R., Guequén, A., Flores, C.A., et al. (2019). Monocarboxylate transporter 4 (MCT4) is a high affinity transporter capable of exporting lactate in high-lactate microenvironments. J. Biol. Chem. *294*, 20135–20147. https://doi.org/10.1074/jbc.RA119.009093.
20. San Martín, A., Ceballo, S., Baeza-Lehnert, F., Lerchundi, R., Valdebenito, R., Contreras-Baeza, Y., Alegría, K., and Barros, L.F. (2014). Imaging mitochondrial flux in single cells with a FRET sensor for pyruvate. PLoS One *9*, e85780. https://doi.org/10.1371/journal.pone.0085780.
21. Polański, R., Hodgkinson, C.L., Fusi, A., Nonaka, D., Priest, L., Kelly, P., Trapani, F., Bishop, P.W., White, A., Critchlow, S.E., et al. (2014). Activity of the monocarboxylate transporter 1 inhibitor AZD3965 in small cell lung cancer. Clin. Cancer Res. *20*, 926–937. https://doi.org/10.1158/1078-0432.CCR-13-2270.
22. Halestrap, A.P. (2013). Monocarboxylic acid transport. Compr. Physiol. *3*, 1611–1643. https://doi.org/10.1002/cphy.c130008.
23. Herzig, S., Raemy, E., Montessuit, S., Veuthey, J.L., Zamboni, N., Westermann, B., Kunji, E.R.S., and Martinou, J.C. (2012). Identification and functional expression of the mitochondrial pyruvate carrier. Science *337*, 93–96. https://doi.org/10.1126/science.1218530.
24. Bricker, D.K., Taylor, E.B., Schell, J.C., Orsak, T., Boutron, A., Chen, Y.C., Cox, J.E., Cardon, C.M., Van Vranken, J.G., Dephoure, N., et al. (2012). A mitochondrial pyruvate carrier required for pyruvate uptake in yeast, Drosophila, and humans. Science *337*, 96–100. https://doi.org/10.1126/science.1218099.
25. Rossiter, N.J., Huggler, K.S., Adelmann, C.H., Keys, H.R., Soens, R.W., Sabatini, D.M., and Cantor, J.R. (2021). CRISPR screens in physiologic medium reveal conditionally essential genes in human cells. Cell Metab. *33*, 1248–1263.e9. https://doi.org/10.1016/j.cmet.2021.02.005.
26. Carcamo-Lemus, N., Rauseo, D., san Martín, A., Lagos, C.F., Barros, L.F., and Sandoval, P.Y. (2025). The MPC is a facultative pyruvate/lactate exchanger. Preprint at bioRxiv. https://doi.org/10.1101/2025.11.29.691055.
27. Chance, B., Williams, G.R., Holmes, W.F., and Higgins, J. (1955). Respiratory enzymes in oxidative phosphorylation. V. A mechanism for oxidative phosphorylation. J. Biol. Chem. *217*, 439–451. https://doi.org/10.1016/S0021-9258(19)57193-9.
28. Reinert, K.C., Gao, W., Chen, G., Wang, X., Peng, Y.P., and Ebner, T.J. (2011). Cellular and metabolic origins of flavoprotein autofluorescence in the cerebellar cortex in vivo. Cerebellum *10*, 585–599. https://doi.org/10.1007/s12311-011-0278-x.
29. Nicholls, D.G., and Ferguson, S.J. (2013). Bioenergetics (Academic Press).
30. Koveal, D., Rosen, P.C., Meyer, D.J., Díaz-García, C.M., Wang, Y., Cai, L.H., Chou, P.J., Weitz, D.A., and Yellen, G. (2022). A high-throughput multiparameter screen for accelerated development and optimization of soluble genetically encoded fluorescent biosensors. Nat. Commun. *13*, 2919. https://doi.org/10.1038/s41467-022-30685-x.
31. Aggarwal, A., Liu, R., Chen, Y., Ralowicz, A.J., Bergerson, S.J., Tomaska, F., Mohar, B., Hanson, T.L., Hasseman, J.P., Reep, D., et al. (2023). Glutamate indicators with improved activation kinetics and localization for imaging synaptic transmission. Nat. Methods *20*, 925–934. https://doi.org/10.1038/s41592-023-01863-6.
32. Arce-Molina, R., Cortés-Molina, F., Sandoval, P.Y., Galaz, A., Alegría, K., Schirmeier, S., Barros, L.F., and San Martín, A. (2020). A highly responsive pyruvate sensor reveals pathway-regulatory role of the mitochondrial pyruvate carrier MPC. eLife *9*, e53917. https://doi.org/10.7554/eLife.53917.
33. Murphy, M.P. (2009). How mitochondria produce reactive oxygen species. Biochem. J. *417*, 1–13. https://doi.org/10.1042/BJ20081386.
34. Pak, V.V., Ezeriņa, D., Lyublinskaya, O.G., Pedre, B., Tyurin-Kuzmin, P.A., Mishina, N.M., Thauvin, M., Young, D., Wahni, K., Martínez Gache, S.A., et al. (2020). Ultrasensitive genetically encoded indicator for hydrogen peroxide identifies roles for the oxidant in cell migration and mitochondrial function. Cell Metab. *31*, 642–653.e6. https://doi.org/10.1016/j.cmet.2020.02.003.
35. Murphy, M.P., Bayir, H., Belousov, V., Chang, C.J., Davies, K.J.A., Davies, M.J., Dick, T.P., Finkel, T., Forman, H.J., Janssen-Heininger, Y., et al. (2022). Guidelines for measuring reactive oxygen species and oxidative damage in cells and in vivo. Nat. Metab. *4*, 651–662. https://doi.org/10.1038/s42255-022-00591-z.
36. San Martín, A., Arce-Molina, R., Galaz, A., Pérez-Guerra, G., and Barros, L.F. (2017). Nanomolar nitric oxide concentrations quickly and reversibly modulate astrocytic energy metabolism. J. Biol. Chem. *292*, 9432–9438. https://doi.org/10.1074/jbc.M117.777243.
37. Zhao, R.Z., Jiang, S., Zhang, L., and Yu, Z.B. (2019). Mitochondrial electron transport chain, ROS generation and uncoupling (Review). Int. J. Mol. Med. *44*, 3–15. https://doi.org/10.3892/ijmm.2019.4188.
38. Gladden, L.B. (2004). Lactate metabolism: a new paradigm for the third millennium. J. Physiol. *558*, 5–30. https://doi.org/10.1113/jphysiol.2003.058701.
39. Ferguson, B.S., Rogatzki, M.J., Goodwin, M.L., Kane, D.A., Rightmire, Z., and Gladden, L.B. (2018). Lactate metabolism: historical context, prior misinterpretations, and current understanding. Eur. J. Appl. Physiol. *118*, 691–728. https://doi.org/10.1007/s00421-017-3795-6.
40. Chen, Y.J., Mahieu, N.G., Huang, X., Singh, M., Crawford, P.A., Johnson, S.L., Gross, R.W., Schaefer, J., and Patti, G.J. (2016). Lactate metabolism is associated with mammalian mitochondria. Nat. Chem. Biol. *12*, 937–943. https://doi.org/10.1038/nchembio.2172.
41. Young, A., Oldford, C., and Mailloux, R.J. (2020). Lactate dehydrogenase supports lactate oxidation in mitochondria isolated from different mouse tissues. Redox Biol. *28*, 101339. https://doi.org/10.1016/j.redox.2019.101339.
42. Hashimoto, T., Hussien, R., Cho, H.S., Kaufer, D., and Brooks, G.A. (2008). Evidence for the mitochondrial lactate oxidation complex in rat neurons: demonstration of an essential component of brain lactate shuttles. PLoS One *3*, e2915. https://doi.org/10.1371/journal.pone.0002915.
43. Zhang, L., Xin, C., Wang, S., Zhuo, S., Zhu, J., Li, Z., Liu, Y., Yang, L., and Chen, Y. (2024). Lactate transported by MCT1 plays an active role in promoting mitochondrial biogenesis and enhancing TCA flux in skeletal muscle. Sci. Adv. *10*, eadn4508. https://doi.org/10.1126/sciadv.adn4508.
44. Halestrap, A.P. (1975). The mitochondrial pyruvate carrier. Kinetics and specificity for substrates and inhibitors. Biochem. J. *148*, 85–96. https://doi.org/10.1042/bj1480085.
45. Thieren, L., Zanker, H.S., Droux, J., Dalvi, U., Wyss, M.T., Waag, R., Germain, P.L., von Ziegler, L.M., Looser, Z.J., Hösli, L., et al. (2025). Astrocytic GLUT1 deletion in adult mice enhances glucose metabolism and resilience to stroke. Nat. Commun. *16*, 4190. https://doi.org/10.1038/s41467-025-59400-2.
46. Mayorek, N., Schlossberg, M., Mansour, Y., Pillar, N., Stein, I., Mushasha, F., Baziza Paz, G., Medvedev, E., Manevitch, Z., Menzel, J., et al. (2025). L-2-hydroxyglutarate regulates centromere and heterochromatin conformation in the male germline. PLoS Genet. *21*, e1011785. https://doi.org/10.1371/journal.pgen.1011785.

47. Williamson, D.H., Lund, P., and Krebs, H.A. (1967). The redox state of free nicotinamide-adenine dinucleotide in the cytoplasm and mitochondria of rat liver. Biochem. J. *103*, 514–527. https://doi.org/10.1042/bj1030514.

48. Poburko, D., and Demaurex, N. (2012). Regulation of the mitochondrial proton gradient by cytosolic Ca(2)(+) signals. Pflugers Arch. *464*, 19–26. https://doi.org/10.1007/s00424-012-1106-y.

49. Li, X., Zhang, Y., Xu, L., Wang, A., Zou, Y., Li, T., Huang, L., Chen, W., Liu, S., Jiang, K., et al. (2023). Ultrasensitive sensors reveal the spatiotemporal landscape of lactate metabolism in physiology and disease. Cell Metab. *35*, 200–211.e9. https://doi.org/10.1016/j.cmet.2022.10.002.

50. Chen, W.W., Freinkman, E., Wang, T., Birsoy, K., and Sabatini, D.M. (2016). Absolute quantification of matrix metabolites reveals the dynamics of mitochondrial metabolism. Cell *166*, 1324–1337.e11. https://doi.org/10.1016/j.cell.2016.07.040.

51. Brooks, G.A. (2009). Cell-cell and intracellular lactate shuttles. J. Physiol. *587*, 5591–5600. https://doi.org/10.1113/jphysiol.2009.178350.

52. Barros, L.F., Fernández-Moncada, I., Marsicano, G., Ruminot, I., Saab, A.S., and Weber, B. (2025). Scale-spanning crosstalk between metabolism and information processing. Cell Metab. *37*, 2303–2310. https://doi.org/10.1016/j.cmet.2025.10.012.

53. Valvona, C.J., Fillmore, H.L., Nunn, P.B., and Pilkington, G.J. (2016). The regulation and function of lactate dehydrogenase A: therapeutic potential in brain tumor. Brain Pathol. *26*, 3–17. https://doi.org/10.1111/bpa.12299.

54. Sada, N., Lee, S., Katsu, T., Otsuki, T., and Inoue, T. (2015). Epilepsy treatment. Targeting LDH enzymes with a stiripentol analog to treat epilepsy. Science *347*, 1362–1367. https://doi.org/10.1126/science.aaa1299.

55. Haspula, D., Vallejos, A.K., Moore, T.M., Tomar, N., Dash, R.K., and Hoffmann, B.R. (2019). Influence of a hyperglycemic microenvironment on a diabetic versus healthy rat vascular endothelium reveals distinguishable mechanistic and phenotypic responses. Front. Physiol. *10*, 558. https://doi.org/10.3389/fphys.2019.00558.

STAR★METHODS

KEY RESOURCES TABLE

REAGENT or RESOURCE	SOURCE	IDENTIFIER
Antibodies		
Rabbit anti-NeuN	Abcam	Cat#177487; RRID: AB_2532109
Goat anti-GFP	Thermo Fisher	Cat#600-101-215M; RRID: AB_3662138
Mouse anti-HSP60	Abcam	Cat#59457; RRID: AB_2121285
Alexa Fluor 647 donkey anti-rabbit	Thermo Fisher	Cat#A32795; RRID: AB_2762835
Alexa Fluor 488 AffiniPure donkey anti-goat	Jackson ImmunoResearch Labs	Cat#705-545-003; RRID: AB_2340428
Cy3 AffiniPure donkey anti-mouse	Jackson ImmunoResearch Labs	Cat#715-165-151; RRID: AB_2315777)
Anti-Kla rabbit	PTM Biolabs	Cat#PTM-1401; RRID: AB_2868521
β-actin	Santa Cruz biotechnology	Cat#sc-47778; RRID: AB_626632
Horseradish peroxidase anti-rabbit	Jackson ImmunoResearch Labs	Cat#711-035-152; RRID: AB_10015282
Bacterial and virus strains		
AAV6/2-hSyn1-chl-Mito-CanlonicSF-WPRE-bGHp	Custom preparation at University of Zurich and UNC Viral Core Facility	N/A
AAV1/2-hSyn1-Laconic-WPRE-hGHp	Custom preparation at University of Zurich and UNC Viral Core Facility	N/A
AAV1/2-hSyn1-eLiLac-WPRE-hGHp	Custom preparation at University of Zurich and UNC Viral Core Facility	N/A
Chemicals, peptides, and recombinant proteins		
Sodium L-lactate	Sigma-Aldrich	L7022; CAS: 867-56-1
Sodium pyruvate	Sigma-Aldrich	P2256; CAS: 113-24-6
Sodium oxamate	Sigma-Aldrich	O2751; CAS: 565-73-1
L-glutamic acid monosodium salt monohydrate	Sigma-Aldrich	49621; CAS: 6106-04-3
L-(-)-malic acid	Sigma-Aldrich	112577; CAS: 97-67-6
AR-C155858	Sigma-Aldrich	5.33436; CAS: 496791-37-8
UK5099	Sigma-Aldrich	5.04817; CAS: 56396-35-1
AZD3965	MedchemExpress	HY-12750; CAS: 1448671-31-5
4-(Chloromercuri) benzenesulfonic acid sodium salt (pCMBS)	Toronto Research Chemicals	TRC-C367750; CAS: 14110-97-5
Syrosingopine	Sigma-Aldrich	SML1908; CAS: 84-36-6
Rotenone	Sigma-Aldrich	R8875; CAS: 83-79-4
Antimycin A	Sigma-Aldrich	A8674; CAS: 1397-94-0
Digitonin	Sigma-Aldrich	D141; CAS: 11024-24-1
BCECF,AM (2′,7′-Bis-(2-Carboxyethyl)-5-(and-6)-Carboxyfluorescein, Acetoxymethyl Ester)	Invitrogen	Cat#B1170
Fluo 4, AM, cell permeant	Invitrogen	Cat#F14201
Rhod-2, AM, cell permeant	Invitrogen	Cat#R1245MP
adenosine 5′ diphosphate sodium salt	Sigma-Aldrich	A2754; CAS: 20398-34-9
cOmplete, EDTA-free Protease Inhibitor Cocktail	Sigma-Aldrich	Cat#11873580001
L-Lactate Assay Kit	Sigma-Aldrich	Cat#MAK329-1KT
Mitochondrial Isolation kit	Sigma-Aldrich	Cat#MITOISO2-1KT
Pierce BCA Protein Assay Kit	Thermo Fisher Scientific	Cat#23225, Cat#23227 and Cat#A65453
ATP magnesium salt	Sigma-Aldrich	A9187; CAS: 74804-12-9
Critical commercial assays		
Lipofectamine 3000 Transfection Reagent	Invitrogen	Cat#L3000015

(*Continued on next page*)

Continued

REAGENT or RESOURCE	SOURCE	IDENTIFIER
Deposited data		
Data in Figures 1, 2, 3, 4, 5, and S1–S5, uncropped western blots and sequence of lactylated proteins in mitochondria.	This study	Mendeley Data as 10.17632/3jcp9t922s.2
Experimental models: Cell lines		
HEK293	ATCC	ATCC-CRL-1573
Hep-G2	ATCC	ATCC-HB-8065
MDA-MB-231	ATCC	ATCC-CRM-HTB-26
Cos-7	ATCC	ATCC- CRL1-651
HEK040: stable cell line for CanlonicSF in mitochondria	Custom preparation at CECs	N/A
HEK024: stable cell line for CanlonicSF in the cytosol	Custom preparation at CECs	N/A
HEK017: stable cell line for Pyronic in mitochondria	Custom preparation at CECs	N/A
MDA021: stable cell line for PyronicSF in mitochondria	Custom preparation at CECs	N/A
Experimental models: Organisms/strains		
Mouse:C57BL/6J x CBA/J	The Jackson Laboratory	JAX: 100011
Recombinant DNA		
pLentiCRISPR-v1-sgMPC2_7	gifted by Jason Cantor	Addgene Plasmid #163457
pLentiCRISPR-v1-sgMPC2_9	gifted by Jason Cantor	Addgene Plasmid #3163458
Plasmid: canlonic	Aburto et al.[11]	Addgene Plasmid #178342
Plasmid: pyronic	San Martín et al.[20]	Addgene Plasmid #51308
Plasmid: pyronicSF	Arce-Molina et al.[32]	Addgene Plasmid #124812
Plasmid: HyPer7.2DAAO-mito	Pak et al.[34]	Addgene Plasmid #168304
Plasmid: LiLac	Koveal et al.[30]	Addgene Plasmid #184570
Plasmid:mito-CanlonicSF	This study	Addgene #224465
Software and algorithms		
Fluoview FV10-ASW 3.0	Olympus	N/A
ImageJ 1.49m	NIH	http://imagej.net

EXPERIMENTAL MODEL AND STUDY PARTICIPANT DETAILS

Animals

Animal handling was carried out in strict accordance with the recommendations in the Guide for the Care and Use of Laboratory Animals of the National Institutes of Health. Procedures in Valdivia were approved by the Centro de Estudios Científicos Animal Care and Use Committee, project 1230145, and sanctioned by the Dirección de Integridad, Seguridad y Ética de la Investigación, Universidad San Sebastián. Primary cultures were obtained C57BL/6J × CBA/J embryos. Procedures in Zurich were approved by the local veterinary authorities according to the guidelines of the Swiss Animal Protection Law, Veterinary Office, Canton of Zurich (Animal Welfare Act 16 December 2005, and Animal Welfare Ordinance 23 April 2008). In vivo measurements were made on female C57BL/6J mice (Charles River) of 8-16 weeks of age (20-27 g bodyweight). All animals were kept in standardized IVC cages with access to water and food at libitum and were subjected to an inverted 12 h light-dark cycle.

Cell lines

Human Embryonic Kidney cells (HEK293), MDA-MB-231, Cos-7, and Hep-G2 cells were purchased from the American Type Culture Collection (ATCC). Cell lines were not authenticated. Cell lines were tested negative for mycoplasma contamination.

METHOD DETAILS

Culture of cell lines

Cultures were passaged with 1% trypsin at 37°C, followed by mechanical disaggregation. HEK293 cells were harvested in DMEM/F12 low glucose plus 10% fetal bovine serum (FBS). MDA-MB-231, Cos-7, and Hep-G2 cells were cultured in Leibovitz medium, high

glucose DMEM and EMEM, respectively. Coverslips were ethanol sterilized and coated with 0.01% poli-L-lysine. Cultures were grown at 37°C in 95% air, 5% CO_2, except for MDA-MB-231, which were cultured in 100% air. Experiments were carried out at 40%-60% confluence.

Reporter cell lines and MPC2KO

Stable cell lines were derived from HEK293 cells by lentiviral bicistronic-vector infection. Cells were subcultured to obtain a final confluence of 40-60%. HEK040 expresses mito-CanlonicSF, HEK024 expresses CanlonicSF (Addgene plasmid #178342) in the cytosol, HEK017 expresses Pyronic (Addgene plasmid #51308) in mitochondria, and MDA021 expresses PyronicSF (Addgene plasmid #124812) in the cytosol. Genetic deletion of the MPC2 was induced by CRISPR/Cas9 edition followed by puromycin (2 ug/ml) selection. The plasmids used for the genetic edition of MPC2 were gifted by Jason Cantor: pLentiCRISPR-v1-sgMPC2_7 (Addgene plasmid # 163457) and pLentiCRISPR-v1-sgMPC2_9 (Addgene plasmid # 163458).

Neural cultures

To obtain cultures enriched in neurons, hippocampus or cortical tissue was extracted from F1 crossover C57BL/6J × CBA/J embryos (18 days). The tissue was dissected from meninges, maintained in an ice-HBSS medium, and enzymatically dissociated with 1% trypsin. After mechanical disaggregation, cells were cultivated in a glass coverslip with neurobasal medium plus 2% B27 supplement, 10 mM glucose, 1% Glutamax, and antibiotics (2.5 mg/ml fungizone and 10 mg/penicillin/streptomycin). The medium was changed every three days, and cells were used after day twelve of cultivation at 95% air and 5% CO_2. For astrocyte enrichment on neuron cultures, the media was supplemented with 3% FBS. To obtain cultures enriched in astrocytes, cortical tissue was extracted from eighteen-day-old embryos (F1 crossover C57BL/6J × CBA/J). The cortex was separated from the meninges, hippocampus, and medulla oblongata and maintained in an ice-HBSS medium for enzymatic dissociation. Cells were grown on coverslips with neurobasal medium plus 10% FBS, 2% B27 supplement, 10 mM glucose, 1% glutamax, and antibiotics (2.5 mg/ml fungizone and 10 mg/ml penicillin/streptomycin). The medium was changed every three days, and cells were used after day eight of cultivation at 95 % air and 5% CO_2.

In vivo assays

Anesthesia. For both surgical interventions and in vivo 2-photon imaging, animals were anesthetized with a mixture of fentanyl (0.05 mg/kg bodyweight; Sintenyl, Sintetica), midazolam (5 mg/kg bodyweight; Dormicum, Roche), and medetomidine (0.5 mg/kg bodyweight; Domitor, Orion Pharma), which was injected subcutaneously (s.c.). Vitamin A ointment (VitA POS, Pharma Medica) was applied to both eyes. Oxygen was supplied throughout anesthesia and animals were kept on a homeothermic blanket until fully recovered.

Headplate implantation, craniotomy, and virus injection. To allow reproducible conditions for in vivo imaging, prior to the craniotomy, a custom-made aluminum head plate was implanted. Mice were fixed in a stereotactic frame (Model 900; David Kopf Instruments). After fur removal, the skin of the scalp was disinfected (Kodan; Schülke & Mayr) and local anesthesia was applied prior to midline incision. The exposed skull was cleaned, and a blue light curable bonding agent applied (Gluma Comfort; Heraeus Kulzer). Next, the head-plate was attached using light-curing dental cement (Tetric EvoFlow; Ivoclar Vivadent). Above the left somatosensory cortex, a craniotomy was performed using a dental drill (OSSEODOC; Bien-Air). Adeno-associated viral vectors (AAVs) were injected intracortically at 350 μm and 150 μm below the dura (80 nl each) by a custom-made micro injector to achieve neuronal sensor protein expression.

The following constructs were used: AAV6/2-hSyn1-chl-Mito-CanlonicSF-WPRE-bGHp (titer: 2.55 x 1012 vg/ml), and (in a subset of mice) additionally AAV1/2-hSyn1-Laconic-WPRE-hGHp (titer: 3.55 x 1012 vg/ml). After virus injections, the brain was covered by a square sapphire glass (3 x 3 mm; 19395-1, Hebo Special Glass), which was sealed with dental cement. In mice used for histology, no headplate was implanted and viral constructs were intracortically injected via 3 small drill holes. For postoperative analgesia, mice were injected s.c. with buprenorphine (0.1 mg/kg bodyweight; Temgesic, Indivior Schweiz AG) and Carprofen (10 mg/kg bodyweight; Rimadyl inj. ad us. vet., Pfizer) directly after surgery and with Carprofen every 12 hours thereafter until fully recovered.

Experimental protocol. For imaging experiments and blood plasma lactate measurements after a baseline of 1 min, a 375 mM sodium L-lactate (L7022, Sigma-Aldrich) solution was injected at 1.5 mmol/kg bodyweight over 3 min intravenously via a tail vein catheter using a manually operated peristaltic pump (Reglo digital ISM831, Ismatec SA). For experiments in which plasma lactate levels were determined, the femoral artery was exposed and cannulated with fine bore polyethylene tubing (0.28 mm ID, 0.61 mm OD; Portex; Smiths Medical). Drops of blood were collected from the arterial catheter and blood plasma lactate was measured using an enzymatic lactate assay (lactate pro-2, Arkray Healthcare, USA) at varying time points during the above-mentioned protocol.

Cerebral in vivo lactate measurements. Mice were imaged 3–4 weeks after virus injection using a custom-built 2-photon laser scanning microscope with a tunable pulsed laser (Chameleon Discovery NX TPC; Coherent) at 920 nm excitation wavelength and equipped with a 16x (N16XLWD-PF, 0.8 NA, Nikon) or 25x water immersion objective (W-Plan-Apochromat 25x/1.05 NA, Olympus). Excitation and emission beam paths were separated by a dichroic mirror (F73-825; AHF Analysentechnik). Emission was further separated by dichroic mirrors at 506 nm (F38-506; AHF Analysentechnik) and at 560 nm (F38-560; AHF Analysentechnik) and was detected with photomultipliers (H9305-03, Hamamatsu) equipped with respective emission filters for blue (F39-477; AHF Analysentechnik), and for green (F37-545; AHF Analysentechnik). During imaging, mice were head-fixed and kept under anesthesia as described above. Anatomical images were acquired at 0.74 Hz and 512 x 512-pixel resolution. Time series for CanlonicSF

measurements alone were acquired at 1.48 Hz (256 x 256-pixel resolution). Experiments comparing CanlonicSF with Laconic signal changes were acquired at 0.53 Hz (256 x 256-pixel resolution) cycling between the two sensor expression areas. All experiments were acquired using ScanImage (r3.8.1; Janelia Research Campus; for 10 min.

Transfection/infection for in vitro sensor expression

Reagents were acquired from Invitrogen. The mix reaction included the plasmid: MitoSypHer (2 μg; Addgene # 48250), lipofectamine 3000 (2 μL), P3000 reagent (2 μL) and Opti-MEM medium (250 μL). Transfection was done at low confluence (25%), followed by 16–24-hour incubation. Mito-CanlonicSF baculoviral particles were generated in the laboratory. Cell lines were incubated for 48 hours before experiments. Astrocyte cultures were infected between the sixth and seventh day for 48 hours with no medium change, and primary neuron cultures were infected between the eighth and ninth day for 72 hours without changing the neurobasal medium. The viral construct for eLiLac expression was designed by cloning the eLilac construct into a viral plasmid for neuronal expression under the hSyn promoter. Viral vectors (AAV6 serotype) were produced by the Viral Vector Facility of UZH and ETH Zurich and are available on the online repository (v1236).

Immunohistochemistry

After three weeks of virus injections, mice were deeply anesthetized with 200 μl pentobarbital (50 mg/ml intraperitoneally; Kantonsapotheke Zürich) and transcardially perfused with artificial cerebrospinal fluid (ACSF, pH 7.4) followed by 2 % paraformaldehyde (PFA, dissolved in 1 X phosphate-buffered saline (PBS), pH 7.4). Following perfusion, the brain was carefully extracted, post-fixed in 4 % PFA for 3 h and subsequently kept in a 30 % sucrose solution (in 1 X PBS, pH 7.4) overnight at 4°C. The fixed tissue was then frozen and cut into 30 μm coronal sections using a cryomicrotome (Hyrax KS 24 microtome; Zeiss, Switzerland). Immunohistochemistry was performed according to standard protocols for staining of fixed, free-floating sections. In short, sections were washed, pre-blocked for 1 h (using normal donkey serum), and then incubated with primary antibodies (see below) overnight at 4°C. The next day, sections were washed, incubated for 45 min with secondary antibodies and DAPI (abcam, 228549), washed again, mounted onto glass slides, and coverslipped with mounting medium (Dako fluorescence mounting medium; Agilent, CA, USA). Images were acquired using a confocal laser scanning microscope (LSM 800; Zeiss, Switzerland) equipped with a 63x objective (Plan-Apochromat, NA 1.4, Oil).

Primary antibodies: rabbit anti-NeuN (abcam, 177487), goat anti-GFP (Thermo Fisher, 600-101-215M), and mouse anti-HSP60 (abcam, 59457). Secondary antibodies: Alexa Fluor 647 donkey anti-rabbit (Invitrogen, A32795), Alexa Fluor 488 AffiniPure donkey anti-goat (Jackson ImmunoResearch Labs, 705-545-03), and Cy3 AffiniPure donkey anti-mouse (Jackson ImmunoResearch, 715-165-151).

Fluorescent dye loading

Dyes were acquired from Sigma-Aldrich. Cultures were incubated in the dark for 10 min at 37°C in BCECF-AM (2 mM, 2000 x), calcein-AM (4 mM, 4000 x) or FLUO-4-AM (4 mM, 4000 x) were diluted in KRH buffer supplemented with 0.02% pluronic F-127. Rhod-2 (40 mM, 100 x) was diluted in KRH buffer supplemented with 5 mM glucose, and cultures were incubated for 15 minutes at 4°C. After removal of the solution, cultured were incubated overnight with culture medium. Cultures were incubated with TMRM (100 μM in DMSO, 2500 x) for 13 minutes.

In vitro imaging

Cells were imaged at room temperature (22–25°C) using an upright Olympus FV1000 confocal microscope equipped with 440, 488 nm and 543 nm laser lines and a 20X water immersion objective (NA 1.0). Alternatively, cells were imaged with an LSM990 Zeiss spectral confocal microscope. Intact cells were imaged in in KRH buffer of the following composition (in mM): 136 NaCl, 3 KCl, 1.25 $CaCl_2$, 1.25 $MgSO_4$, 10 HEPES pH 7.4. For permeabilization, cultures were perfused for 3 min with 30 μM digitonin and 200 μM ADP in intracellular buffer (mM): 130 KCl, 10 NaCl, 1.25 $MgCl_2$, 0.37 $CaCl_2$, 1 EGTA, 10 HEPES at pH 7.20. Estimated free Ca^{2+} in this solution is 90 nM (Maxchelator). Digitonin was washed out for at least 10 minutes in intracellular buffer. Osmolarity of the buffers was between 270 and 275 mOsm/L. NAD(P)H autofluorescence was measured with an Olympus BX61W1 microscope equipped with a 20X water-immersion objective, a CAIRN monochromator and a Rollera camera controlled with MetaFluor software.

Sensor and fluorescent dye imaging. CanlonicSF, PyronicSF, calcein and FLUO-4 were imaged at 488 nm excitation, 515 ± 10 nm emission. eLiLac was imaged 440 nm excitation/480 ± 15 emission. HyPer7.2 was imaged at 488 nm excitation, 610 ± 50 nm emission. Mito-SyPher and BCECF were excited sequentially at 440 nm and 488 nm, with both emissions collected at 515 ± 10 nm. Pyronic was imaged at 440 nm excitation/480 ± 15 nm and 550 ± 15 emissions. For ratiometric purposes, accompanying red proteins were imaged at 543 nm excitation, 610 ± 50 nm emission. Flavoprotein autofluorescence was measured at 488 excitaction, 515 ± 10 nm emission. For NAD(P)H autofluorescence cells were excited at 360 nm excitation and emission was collected with a 420-480 nm band-pass filter.

Calibration of mito-CanlonicSF

A multiplate reader (Perkin Elmer) was used to determine mito-CanlonicSF K_D in mitochondria. HEK040 were cultured in 96 well plates and permeabilized under glutamate 0.2 and malate 0.1 mM. First reads correspond to nominal zero (6 mM of oxamate) and second reads involved curves dose-response of lactate with or without 1 μM of FCCP. Lactate concentrations were (mM): 0.0375,

0.07, 0.1, 0.3, 0.6, 1.2, 2.4, 10, 20 and 100. Each well was excited at 488 and 543 nm. The ratio of the emission length was obtained, and the data was normalizing with the first reads. The average of each dose was calculated, processed in percentage (%). A rectangular hyperbola was fitted to the date to obtain the K_D.

Extracellular lactate determination

HEK040 cells grown in a 10 cm dish at 70% confluency were detached by gentle pipetting using KRH buffer supplemented with 2 glucose, 1 lactate, and 0.1 pyruvate. Cells were collected by centrifugation (800g for 1 min) and permeabilized for 3 min in intracellular buffer containing 30 μM digitonin and 0.2 mM ADP. After three washes, cells were incubated for 1 h at 37 °C in the absence or presence of 0.1 mM pyruvate, 0.2 mM glutamate, 0.1 mM malate. Lactate in the supernatant was quantified using a colorimetric assay, according to the manufacturer's instructions. For protein determination, cell pellets were incubated in 500 μL of lysis buffer (50 mM Tris, 150 mM NaCl, 1 mM EDTA, 1% Triton X-100, pH 7.5) with protease inhibitors. Lysates were centrifuged (14,000g, 20 min, 4 °C), and protein concentration in the supernatants was determined using a BCA assay.

Mitochondrial isolation

HEK293 cell mitochondria were isolated using a commercial isolation kit (MITOISO2) suitable for functional analysis,[55] according to the manufacturer protocol. Cells grown in three 10 cm dishes were collected at ~90% confluency, washed with PBS, and detached with trypsin–EDTA. Cell pellets were washed twice in ice-cold PBS and resuspended in 1× Extraction Buffer A supplemented with protease inhibitors. Briefly, after a 10–15 min incubation on ice, cells were mechanically disrupted with 90 strokes through a 25G blunt needle followed by 90 strokes in a chilled Dounce homogenizer. The homogenate was cleared by centrifugation at 600 × g for 10 min at 4°C, and the resulting supernatant was centrifuged at 11,000 × g for 10 min at 4°C to obtain the crude mitochondrial pellet. Mitochondria were resuspended either in intracellular buffer with EDTA-free protease inhibitor cocktail (cOmplete) for functional assays or in CelLytic M supplemented with protease inhibitors for protein extraction. The quality of the preparation was assessed by immunodetection of VDAC and beta-actin, as illustrated in Figure 1E.

Lactate determination in the supernatant of isolated mitochondria

Lactate levels were quantified using the colorimetric lactate assay kit (MAK329) according to the manufacturer's instructions. Lactate standards (0–2 mM) were prepared in intracellular buffer supplemented with 1× EDTA-free protease inhibitor cocktail (cOmplete) and contained 0.5 mM glutamate and 0.5 mM malate. Crude mitochondria and mocks were incubated for 1 h at 37°C in intracellular buffer with 1× EDTA-free protease inhibitor cocktail, 0.5 mM glutamate, 0.5 mM malate, 0.5 mM pyruvate and 0.5 mM lactate. Mock controls included the same substrates without mitochondria. After incubation, samples were centrifuged (12,000 × g, 10 min, 4°C), and supernatants were collected for lactate quantification. Reaction mix was prepared following the kit protocol and added to 10 μL of sample or standard in 384-well plates. Absorbance at 565 nm was recorded immediately and after 20 min at room temperature. Lactate concentrations were determined from standard curves.

Lactylation analysis

Western blotting

HEK293 cells ($2x10^6$) were treated in the presence or absence of lactate. Cells were resuspended (1X PBS) in agitation and centrifuged at 850g for 2 minutes (2X). Mitochondrial fractioning was performed by density gradient centrifugation. The fraction was lysed in RIPA (1% SDS + 1% deoxycholate and 1% triton), re-suspended in 100 uL of RIPA modified buffer and vortexed for 1 min. Proteins were quantified by QuantiPro BCA Assay Kit (Sigma Aldrich, QPCA-1KT) and 15 μg of protein were loaded per well. Gel electrophoresis was carried out in polyacrylamide 6% and 12%. First antibody, Anti Kla rabbit 1:5000 (PTM Biolabs, catalog N° PTM-1401), was maintained in agitation overnight at 4°C. The second antibody, Horseradish peroxidase-conjugated 1:10000, was incubated at 37°C for 1 hour (catalog N° 711-035-152. West Femto Maximal Sensitivity substrate (peroxidase) (Thermo Fisher catalog N° 34095) was used for chemiluminescence visualization. β-actin (Santa Cruz biotechnology C4, catalog N° sc-47778) was blotted as an internal control. Western blot images were processed in Fiji, with identical selection areas applied to each band to enable comparisons. Band intensity, expressed as area under the curve, was normalized to β-actin.

Proteomics

HEK293 cells ($2x10^6$) were used for the control and lactate-treated samples. Cells were lysed in 8M Urea, 100 mM NaCl, 50 mM ammonium bicarbonate (ABC) and 1X protease inhibitor (complete Protease Inhibitor Cocktail, Roche). Sonication was performed by 10 cycles of 10 seconds each, one minute of rest. Cells were sedimented at 15,000g for 15 min. The supernatants were collected and quantified using the Dual-Range BCA Protein Assay kit (ThermoFisher). Proteins (100μg) were reduced with dithiothreitol 20 mM (30 min, 60°C) and alkylated with iodoacetamide 40 mM (15 min, room temperature in darkness). The samples were treated with urea (0,6 M) and trypsin in a ratio 1:50 with overnight agitation at 37°C. After 16h the reaction was stopped with trifluoroacetic acid (TFA). The digested proteins (200 μg) were used for immunoprecipitation using anti-Kla antibody coupled to ProtA/G-beads (Santa Cruz). Antibody was coupled to ProtA/G-beads overnight at 4°C in agitation and washed-out (3X) 24 hours later with ETN buffer (NaCl 3M, EDTA 0,1M and TRIS 1,5M, pH 8,0). The digested peptides were added and incubated for 6 hours at 4°C in agitation. Immunocomplexes were washed with ETN buffer (3X) and with ultrapure water (2X). Peptides were eluted using TFA 1% and cleaned-up using Pierce C18 Spin Columns (ThermoFisher).

For nHPLC-MS/MS analysis tryptic peptides (500 ng) were separated using an Easy nLC II liquid chromatograph and analyzed on a Q Exactive Plus mass spectrometer. Peptides were resolved using a C18 PepMap Easy-Spray reverse-phase column (75μm x15cm) with a particle size of 3μm in a gradient of 6-35% ACN over 50 minutes for proteome and 30 minutes for immunoprecipitation, followed by 35-45% over 15 minutes at a flow rate of 200nl/min for a total run of 98-minutes for the proteome and 78-minutes for immunoprecipitation analyses were used. The parameters were set using Xcalibur acquisition software (version 4.2). Spectra were obtained using the Orbitrap analyzer in FullMS mode within a range of 300-1800m/z at a resolution of 70,000. The 20 and the 5 most intense ions were selected for fragmentation in the proteome and the immunoprecipitation, respectively. dd-MS2 spectra were acquired at resolution of 17,500. The target value was set to 1x105 with an isolation window of 1.8m/z. The maximum injection time was set to 100 msec with a normalized collision energy of 28eV.

Database search

Spectra were searched against UniProtKB/Swiss-Prot database search restricted to Homo sapiens (released on 04/2022, with 20374 entries), using PEAKS Studio software (version 10.6) with a parent/fragment mass error tolerance of 10ppm/0.02Da. Potential false positives were filtered using a 1% False Discovery Rate (FDR). Variable proteome modifications included Oxidation (M), Pyro-glu form E, Pyro-glu form Q, Deamidation (NQ) and Lactylation (K) (+72.02 Da). The subcellular location of mitochondrial proteins was identified by using UniProtKB/Swiss-Prot database search.

Image Processing

Data is obtained from sequential images and managed in Fiji. The background or noise was substracted in each photo of every channel. Due to the low-resolution on which the light was captured to increase temporal resolution, a mitochondrial mask was applied. This mask allows thresholding of the fluorescent signal for each channel in a specific pixel range to avoid outliers and dismiss noisy brilliance. The final outcome of the mask assigned a value of zero to those very low signals and was acquired as integrated density.

QUANTIFICATION AND STATISTICAL ANALYSIS

Data are expressed as mean ± SEM or Box-and-Whisker plots indicating percentiles 10, 25, 50, 75 and 90. Data analysis was performed in Sigma Plot software. A paired t-test was applied to ascertain differences in before-after treatment protocols with normal distribution. In case of failed normality test (Shapiro-Wilk), differences were assigned with the Mann Whitney-Wilcoxon signed rank test (pairs). *, $p < 0.05$. Not significant (NS), $p > 0.05$).